

BayesTime: Bayesian Functional Principal Components for Sparse Longitudinal Data

Lingjing Jiang¹, Yuan Zhong², Chris Elrod³, Loki Natarajan¹,
Rob Knight^{4,5,6,7}, Wesley K. Thompson¹

¹Herbert Wertheim School of Public Health and Human Longevity Science, University of California San Diego, La Jolla, CA

²Department of Biostatistics, University of Michigan, Ann Arbor, MI

³Julia Computing, Boston, MA

⁴Department of Pediatrics, University of California San Diego, La Jolla, CA

⁵Center for Microbiome Innovation, University of California San Diego, La Jolla, CA

⁶Department of Computer Science and Engineering, University of California San Diego, La Jolla, CA

⁷Department of Bioengineering, University of California San Diego, La Jolla, CA

February 6, 2022

Abstract

Modeling non-linear temporal trajectories is of fundamental interest in many application areas, such as in longitudinal microbiome analysis. Many existing methods focus on estimating mean trajectories, but it is also often of value to assess temporal patterns of individual subjects. Sparse principal components analysis (SFPCA) serves as a useful tool for assessing individual variation in non-linear trajectories; however its application to real data often requires careful model selection criteria and diagnostic tools. Here, we propose a Bayesian approach to SFPCA, which allows users to use the efficient leave-one-out cross-validation (LOO) with Pareto-smoothed importance sampling (PSIS) for model selection, and to utilize the estimated shape parameter from PSIS-LOO and also the posterior predictive checks for graphical model diagnostics. This Bayesian implementation thus enables careful application of SFPCA to a wide range of longitudinal data applications.

Keywords: Sparse Longitudinal Data; Functional Data Analysis; Dimension Reduction; Temporal Pattern; Microbiome

1 Introduction

Longitudinal data, i.e., multiple observations collected on the same subject over time, are ubiquitous in biomedical research. In addition to using longitudinal data to estimate mean trajectories, it is often of great interest to characterize individual subject variation. Both the mean trajectory and individual subject deviations from the mean trajectory may be highly non-linear and hard to characterize using typical modeling approaches for longitudinal data such as linear mixed-effects models. Additionally, longitudinal data are often collected at irregular timing and frequency across subjects (they are “sparse”), and methods for estimating trajectories need to be able to handle this common scenario.

For example, a question of fundamental interest in microbiome research is how the microbiome evolves in individual subjects as a response to subject-level perturbations, such as disease, diet and lifestyle (Kostic et al., 2015; Halfvarson et al., 2017; Smarr et al., 2017; Weingarden et al., 2015; David et al., 2014; Turnbaugh et al., 2009; Fierer et al., 2008). Accurate continuous monitoring of a subject’s microbiome may substantially improve prevention and treatment of some disorders. However, high-density temporal sampling is not currently feasible for microbiome studies; in practice, microbiome samples are collected infrequently and irregularly across time and subjects. Moreover, next generation sequencing techniques used to obtain estimates of microbial measurements are noisy, thus further hindering inference regarding the temporal evolution of a given subject’s microbial status. Finally, the microbiome exhibits highly nonlinear dynamics over time, which introduces an additional complication to traditional longitudinal analysis methods. While several analytical methods have been developed to model microbiome temporal dynamics addressing these challenges (Ridenhour et al., 2017; Gibson and Gerber, 2018; Silverman et al., 2018; Shenhav et al., 2019; Silverman et al., 2019), by and large the focus has been on mean trajectories, substantially ignoring potentially important information about variation in trajectories across subjects. Since microbiome progression is highly idiosyncratic, it would be of great interest to capture relevant individual deviation from the mean trajectories, perhaps resulting in personalized predictions and clustering of subjects based on progression patterns.

Sparse functional principal components analysis (SFPCA) serves as a useful tool to estimate smooth mean trajectories while at the same time estimating smooth principal modes of variation of subject-level trajectories around the mean trajectory. SFPCA can be framed as an extension of linear random-effects models, where time effects are treated as random and non-linearity is achieved by choice of the functional basis (James et al., 2000; Kidziński and Hastie, 2018). The covariance structure of the trajectories is modeled as a low-rank matrix to produce efficient estimates of individual trajectories. Various fitting approaches, such as the EM algorithm, kernel smoothing and Newton-Raphson algorithm, have been proposed to estimate parameters of the SFPCA model (James et al., 2000; Yao et al., 2005; Peng and Paul, 2009). These approaches then use model selection techniques, such as cross-validation, Akaike information criterion (AIC) and leave-one-curve-out cross-validation, to select the dimension of basis and the number of principal components. However, due to their reliance on assumptions such as normally-distributed component scores and residuals, these models need to be carefully examined when applied to real data (Kidziński and Hastie, 2018).

We implemented the SFPCA model in a Bayesian framework to provide a flexible modeling approach that incorporates effective model selection and graphical diagnostic methods. Our **BayesTime** R package implementing the Bayesian SFPCA model allows users to use leave-one-out cross-validation (LOO) with Pareto-smoothed importance sampling (PSIS) for model selection (Vehtari et al., 2017), and to utilise the estimated shape parameter from PSIS-LOO and graphical posterior predictive checks for model diagnostics (Gelman et al., 1996; Gabry et al., 2019). This Bayesian implementation thus offers a flexible and comprehensive solution to real-date SFPCA applications, such as longitudinal microbiome data.

The Bayesian framework of SFPCA with PSIS-LOO is described in Section 2, and is implemented in the **BayesTime** package in R (Section 3). Section 4 presents Monte Carlo simulations evaluating the Bayesian SFPCA model performance and further illustrates its use on a real longitudinal microbiome dataset, showing how individual microbiome trends can be visualized and explored with **BayesTime**. Future work is discussed in Section 5.

2 Methods

2.1 Sparse Functional Principal Components Analysis

The classical assumption of functional data analysis is that each trajectory is sampled over a dense grid of time points common to all individuals (Ramsay and Silverman, 2007). However, in practice, trajectories are often measured at an irregular and sparse set of time points that can differ widely across individuals. To address this scenario, James et al. (2000) proposed *sparse functional principal components analysis* (SFPCA) using a reduced rank mixed-effects framework. Let $Y_i(t)$ be the measurement at time t for the i th individual, $\mu(t)$ the overall mean function, f_j the j th principal component function and $\mathbf{f} = [(f_1, f_2, \dots, f_k)]^T$, where k is the number of principal components. Then the James et al. (2000) SFPCA model is given by

$$Y_i(t) = \mu(t) + \sum_{j=1}^k f_j(t)\alpha_{ij} + \epsilon_i(t), \quad i = 1, \dots, N \quad (1)$$

subject to the orthogonality constraint $\int f_j f_l = \delta_{jl}$, the Kronecker δ . The vector $\boldsymbol{\alpha}_i = (\alpha_{i1}, \dots, \alpha_{ik})^T$ is the component weights for the i th individual and $\epsilon_i(t)$ is a normally-distributed residual, independent across subjects and across times within subject. The functions μ and \mathbf{f} are approximated using cubic splines to allow for a smooth but flexible fit. Let $\mathbf{b}(t)$ be a cubic spline basis with dimension $q > k$. The spline basis is orthonormalized so that $\int b_j b_l = \delta_{jl}$. Let Θ and $\boldsymbol{\theta}_\mu$ be, respectively, a $q \times k$ matrix and a q -dimensional vector of real-valued coefficients. For each individual i , denote their measurement times by $\mathbf{t} = (t_{i1}, t_{i2}, \dots, t_{in_i})^T$, and let $\mathbf{Y}_i = (Y_i(t_{i1}), \dots, Y_i(t_{in_i}))^T$ be the corresponding real-valued observations. Then $B_i = (\mathbf{b}(t_{i1}), \dots, \mathbf{b}(t_{in_i}))^T$ is the $n_i \times q$ spline basis matrix for the i th individual. The reduced rank model can then be written as

$$\begin{aligned} Y_i &= B_i \boldsymbol{\theta}_\mu + B_i \Theta \boldsymbol{\alpha}_i + \epsilon_i, \quad i = 1, \dots, N, \\ \Theta^T \Theta &= I, \quad \boldsymbol{\alpha}_i \sim N(0, D), \quad \epsilon_i \sim N(0, \sigma_\epsilon^2 I_{n_i}), \end{aligned} \quad (2)$$

where the covariance matrix D is restricted to be diagonal and I_{n_i} is the $n_i \times n_i$ identity matrix.

2.2 Bayesian SFPCA

We developed the SFPCA model in a Bayesian framework to allow for flexible prior specification and implementation of model selection and assessment methods. We implemented this Bayesian model using Hamilton Markov Chain Monte Carlo (MCMC) sampling algorithm in **Stan** (Carpenter et al., 2017). The real-valued observations $Y_i(t)$ are first standardized to have mean zero and standard deviation one. The prior distributions for parameters in Eq. (2) were chosen as follows:

$$\begin{aligned}\boldsymbol{\theta}_\mu &\sim N_q(0, I_q) \\ \boldsymbol{\alpha}_i &\sim N_k(0, I_k) \\ \boldsymbol{\Theta}_j &\sim N_q(0, I_q), j = 1, \dots, k \\ \epsilon_i &\sim N_{v_i}(0, \sigma_\epsilon^2 I_{v_i}) \\ \sigma_\epsilon &\sim \text{Cauchy}(0, 1),\end{aligned}$$

where $\boldsymbol{\Theta}_j$ is the j th column of the loading matrix $\boldsymbol{\Theta}$, and v_i is the total number of visits for the i th subject. The Bayesian implementation also enables use of leave-one-out cross-validation with Pareto-smoothed important sampling (PSIS-LOO) (Vehtari et al., 2017) to perform model selection on the number of principal components k and the number of basis functions q . Moreover, model fit can be assessed via diagnostics plots from PSIS-LOO as well as the graphical posterior predictive checks obtained from simulating posterior predictive data (Gelman et al., 1996; Gabry et al., 2019).

One difficulty in implementing the Bayesian SFPCA model is that the principal component loadings $\boldsymbol{\Theta}$ are not uniquely specified. For a given $k \times k$ rotation matrix P , if $\boldsymbol{\Theta}^* = \boldsymbol{\Theta}P$ and $\boldsymbol{\Theta}$ obeys the constraints in Eq.(2), then $\boldsymbol{\Theta}^{*T}\boldsymbol{\Theta}^* = P^T\boldsymbol{\Theta}^T\boldsymbol{\Theta}P = I$, and hence $\boldsymbol{\Theta}$ is unidentifiable without additional restrictions. Instead of directly enforcing orthonormality when sampling from the conditional posteriors in the Bayesian model fitting, we sampled the parameters with no constraint on $\boldsymbol{\Theta}$ and then performed a *post hoc* rotation for each iteration of the MCMC algorithm to meet the orthonormality constraint. Since the symmetric matrix $\boldsymbol{\Theta}^T\boldsymbol{\Theta}$ is identifiable and non-negative definite, we applied an eigenvalue decomposition $\boldsymbol{\Theta}^T\boldsymbol{\Theta} = VSV^T$, where V is the $q \times q$ matrix of orthonormal eigenvectors, and

S is the diagonal matrix of eigenvalues, with the q positive eigenvalues ordered from largest to smallest. Let $\Theta^* = V_k$ denote the $q \times k$ matrix consisting of the first k eigenvectors of V , which satisfies $\Theta^{*T}\Theta^* = I$. Finally, we rotated the FPC scores α_i to obtain $\alpha_i^* = \Theta^{*T}\Theta\alpha_i$, so that $\Theta^*\alpha_i^* = \Theta\alpha_i$.

2.3 Model Selection with PSIS-LOO

Leave-one-out cross-validation(LOO) with Pareto smoothed importance sampling (PSIS) is a stable model selection procedure which has been shown to be more robust in the presence of influential observations than other widely used criteria such as AIC (Akaike information criterion), DIC (deviance information criterion) and WAIC (widely applicable information criterion) (Vehtari et al., 2017). In Bayesian leave-one-out cross-validation, the estimate of the out-of-sample predictive fit (expected log pointwise predictive density) is defined as

$$elpd_{loo} = \sum_{i=1}^n \log p(y_i|y_{-i}), \quad (3)$$

where $p(y_i|y_{-i}) = \int p(y_i|\theta)p(\theta|y_{-i})d\theta$ is the leave-one-out predictive density given the data without the i th data point. Typically, LOO-CV requires re-fitting the model n times; however, a computational shortcut exists to enable only one model evaluation. As noted by Gelfand et al. (1992), if the n points are conditionally independent in the data model, we can then evaluate $p(y_i|y_{-i})$ with draw θ^s from the full posterior $p(\theta|y)$ using importance ratios, defined as

$$r_i^s = \frac{1}{p(y_i|\theta^s)} \propto \frac{p(\theta^s|y_{-i})}{p(\theta^s|y)}. \quad (4)$$

However, the posterior $p(\theta|y)$ is likely to have a smaller variance and thinner tails than the leave-one-out distribution $p(\theta|y_{-i})$, and thus a direct use of the formula above induces instability, because the importance ratios can have high or infinite variance.

Vehtari et al. (2015) improve the LOO estimate using Pareto smoothed importance sampling (PSIS), which applies a smoothing procedure to the importance weights. As the distribution of the importance weights used in LOO may have a long right tail, the empirical Bayes estimate of Zhang and Stephens (2009) can be used to fit a generalized Pareto distribution to the tail (e.g. 20% largest importance ratios), and this is done

separately for each held-out data point i . So for each i , the result is a vector of weights $\tilde{w}_i^s = F^{-1}\left(\frac{z-\frac{1}{2}}{M}\right)$, $z = 1, \dots, M$, where M is the number of simulation draws used to fit the Pareto distribution (in this case, $M = 0.2S$), and F^{-1} is the inverse-CDF of the generalized Pareto distribution. Then each vector of weights is truncated at $S^{3/4}\bar{w}_i$, denoted as w_i^s . These results can then be combined to compute the PSIS estimate of the LOO expected log pointwise predictive density:

$$elppd_{\widehat{psis-loo}} = \sum_{i=1}^n \log \frac{\sum_{s=1}^S w_i^s p(y_i|\theta^s)}{\sum_{s=1}^S w_i^s}. \quad (5)$$

2.4 Model Diagnostics

PSIS-LOO is not only efficient, it can also provide useful diagnostics for model checking. The estimated shape parameter \hat{k} of the fitted Pareto distribution can be used to assess the reliability of the estimate; this diagnostic approach can be used routinely with PSIS-LOO for any model with a factorizable likelihood. If $k < \frac{1}{2}$, the variance of the raw importance ratios is finite, the central limit theorem holds, and the estimate converges quickly. If $k \in [\frac{1}{2}, 1]$, the variance of the raw importance ratios is infinite but the mean exists, the generalized central limit theorem for stable distributions holds, and the convergence of the estimate is slower. If $k > 1$, the variance and the mean of the raw ratios distribution do not exist. Vehtari et al. (2017) suggested that if the estimated tail shape parameter \hat{k} exceeds 0.5, the user should be warned, although in practice they have observed good performance of values of \hat{k} up to 0.7. Hence, this threshold of 0.7 could be used in practice for model diagnostics. If the i th LOO predictive distribution has a large \hat{k} value when holding out data point i to evaluate predictive density, it suggests that data point i is a highly influential observation that deserves further examination.

Moreover, since we are implementing a Bayesian SFPCA model, we can also compare the observed data to simulated data from the posterior predictive distribution (Gabry et al., 2019). The idea behind posterior predictive checks is simple: if a model is a good fit, then it should be able to generate data that resemble the observed data. The data used for posterior predictive checks are simulated from the posterior predictive distribution

$p(\tilde{y}|y) = \int p(\tilde{y}|\theta)p(\theta|y)d\theta$, where y is the current observed data, \tilde{y} is the new data to be predicted, and θ are model parameters. By comparing the observed and replicated data in the posterior predictive checks, we may find a need to extend or modify the model.

3 Implementation

The Bayesian SFPCA method has been implemented in R in the `BayesTime` package at github.com/biocore/bayestime. The user can choose a range of the number of principal components and the dimension of cubic spline basis (i.e. the number of internal knots + 4) by the `PC_range` and `nknot_range` argument in `stan_fit` function, with which the knots are placed by the quantile of the time range in the default setting. The following model comparisons are performed with the `optimal_model` function, which compare models based on their $\widehat{elpd}_{psis-loo}$ and standard errors. Moreover, model diagnostics on the chosen model can be visualized using `plot_k_diagnostic` and `plot_posterior_diagnostic` functions.

```
library(BayesTime)
# use PSIS-L00 for model selection
sfpca_stan_results <- stan_fit(sfpca_data = dat, Nsamples = 1000, Nchain
  = 3, Ncores=3, PC_range = c(1,2,3), nknot_range = c(1,2))
optimal_model_idx <- optimal(model_list = sfpca_stan_results)
optimal_model <- sfpca_stan_results[[optimal_model_idx]]
# model diagnostics with Pareto shape parameter k
plot_k_diagnostic(dat, optimal_model)
# model diagnostics with posterior predictive checking
plot_posterior_diagnostic(dat, optimal_model)
```

4 Examples

Using the `BayesTime` package, we evaluated the performance of the Bayesian SFPCA model in Monte Carlo simulation studies and applied it to a longitudinal microbiome dataset to demonstrate its utility in a practical example. Data and code for simulations and real data application are available at <https://github.com/knightlab-analyses/BayesTime-analyses>.

4.1 Simulation Studies

Due to potential sequencing errors and sample collection procedures, missing data and dropouts are the norm rather than the exception in longitudinal microbiome studies. Moreover, despite large-scale cross-sectional microbiome studies such as the Human Microbiome Project (Turnbaugh et al., 2007; Methé et al., 2012) and American Gut Project (McDonald et al., 2018), studies characterizing human-associated microbial communities over time often have relatively small sample sizes (Dethlefsen and Relman, 2011; Flores et al., 2014; Caporaso et al., 2011). Hence, it is important to assess the performance of Bayesian SF-PCA in simulations with various sample sizes and with different levels of sparsity. In our simulations, we varied the total number of subjects at 100, 50, 25, 10, and the proportion of missing values at 0%, 20%, 50% and 80% (i.e., the percentage of randomly deleted observations to create increasingly sparse functional datasets) over observations at 10 time points. To better mimic the reality, we simulated longitudinal trajectories based on an SFPCA model using parameters initially estimated from the real microbiome data in the following way:

1. applying SFPCA to a real longitudinal microbiome dataset (Dominguez-Bello et al., 2016);
2. selecting the optimal number of PCs k and dimension of basis q using PSIS-LOO;
3. extracting the estimated values for population mean curve (θ_μ), FPC loadings (Θ), diagonal covariance matrix of FPC scores (D), and error variance (σ^2).

Then we simulate the data by varying the number of subjects, the number of time points and proportion of missing data as follows:

1. choosing the total number of subjects (N) and of time points (N_T) in order to place possible time points between $[0, 1]$;
2. specifying the average number (μ_T) of time points across all subjects in order to vary the proportion of missing data (approximated as $1 - \mu_T/N_T$) by simulating the observed number of time points for each individual with $n_i \sim \text{Poisson}(\mu_T)$ and then

randomly placing the observed time points in the possible time locations (chosen in the previous step);

3. generating the cubic spline basis matrix $b(t)$ for each subject (orthonormality obtained through Gram-Schmidt orthonormalization);
4. simulating for each subject FPC scores $\alpha_i \sim N(0, D)$ and noise $\epsilon_i \sim N(0, \sigma^2 I)$;
5. obtaining the temporal trajectory for each individual with $Y_i(t) = B_i \theta_\mu + B_i \Theta \alpha_i + \epsilon_i$, where $B_i = (b(t_{i1}), \dots, b(t_{in_i}))^T$
6. repeating steps 1 – 5 100 times for each simulation scenario with different number of subjects and proportion of missing data, thus generating 1600 simulated datasets in total.

Before describing the simulation results, we want to use the scenario of 100 subjects with 80% missing data to demonstrate how to perform model selection with PSIS-LOO and how to use its estimated shape parameter \hat{k} to assess the reliability of the model. Models are compared based on their values of $\widehat{elppd}_{psis-loo}$: the larger the value, the better the model is. Among nine models tested (with the number of PCs and the number of internal knots ranging from 1 to 3), the model with two PC's and one internal knot had the highest $\widehat{elppd}_{psis-loo}$. The second best model (with three PC's and one internal knot) is lower in $\widehat{elppd}_{psis-loo}$ by 1.86, and the standard error of the difference between the two models is 2.21, indicating that the second model provides a similarly good fit. But since the first model is more parsimonious and all of its estimated shape parameters \hat{k} are smaller than 0.7 (Figure 1A), we chose this as our best model.

We also generated graphical displays comparing observed data to simulated data from the posterior predictive distribution. In Figure 1B, the dark line is the distribution of the observed outcomes y and each of the lighter lines is the kernel density estimate of one of the replicates of y from the posterior predictive distribution. This figure shows that there is very little discrepancy between real and simulated data from the model, confirming the model validity for this application.

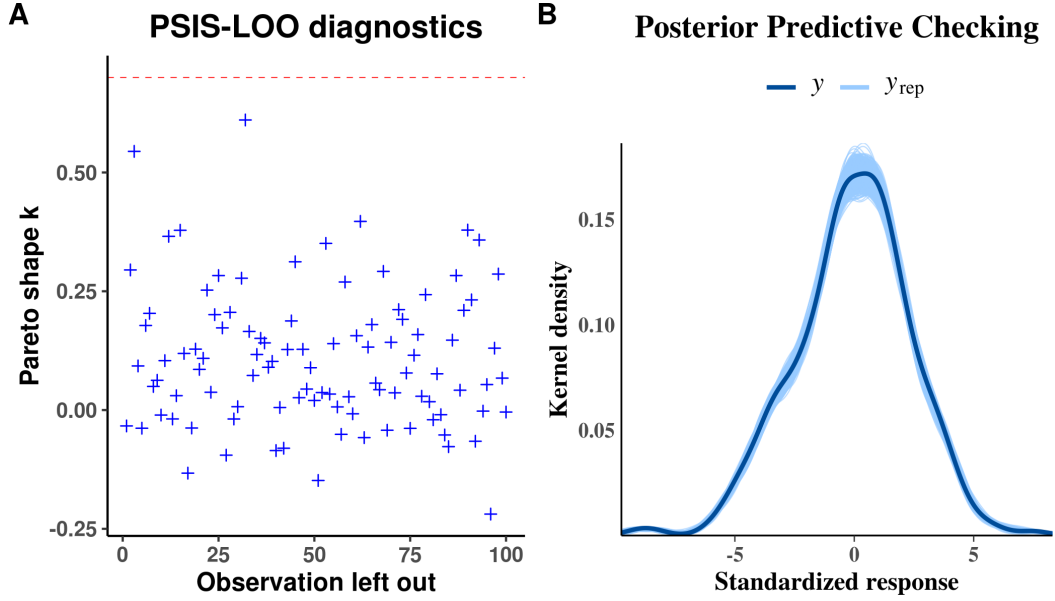


Figure 1: Graphical model checking with PSIS-LOO diagnostic plot and posterior predictive checks for Bayesian SFPCA simulated scenario of 100 subjects with 80% missing data. (A) Scatterplot of estimated Pareto shape parameter \hat{k} in PSIS-LOO diagnostic plot: all \hat{k} 's are lower than the warning threshold 0.7. (B) Graphical posterior predictive checks: kernel density estimate of the observed dataset y (dark curve), with kernel estimates for 100 simulated datasets y_{rep} drawn from the posterior predictive distribution (thin, lighter lines).

To evaluate the performance of Bayesian SFPCA, we investigated how well it recovered the mean trajectory and two PC functions. With 100 subjects, even as the proportion of missing data increased from 0% to 80%, the estimated overall mean curves and PC curves accurately recovered the ground truth in both scenarios (Figure 2). For the scenarios with 50 or 25 subjects with 80% missing data, the estimated mean curves were still close to the ground truth, except for a slight deviation at the two ends due to the large proportion of missing data there (Figure 3A, B). The PC curves were estimated well for both cases on two PCs, despite slight underestimation toward the end on both PCs (Figure 3C, D). As for the challenging scenarios of 10 samples with 50% or 80% missing data, the estimated mean curves in both scenarios and the PC curves for the scenario with 50% missingness were still robust (Figure 4A, B, C). However, for the case with 80% missing data, the estimated PC 1 curve did not capture the decreasing trend as accurately as before and displayed an artificial curvature towards the end; the estimated PC 2 curve also exhibited some deviations from the ground truth (Figure 4D). A closer look at the simulated trajectories (Figure 4B) indicated that few trajectories exhibited the decreasing trend at the beginning in both PCs due to the loss of data, hence the deviated estimation was caused by the limitation of the underlying data. Note that the visual comparisons above were demonstrated using one representative case from each simulation scenario. Results over all 100 simulated datasets for each scenario were summarized in table 1 and 2, showing that in the estimations of both mean (θ_μ) and FPC spline coefficients (Θ), mean squared errors increase as sample size decreases at each given missing proportion, although the variabilities are still within the 95% credible intervals. Moreover, errors for the mean and FPC estimations remain similar despite increasing missing proportion at fixed sample size. In summary, the performance of Bayesian SFPCA is robust to limited sample size and a high proportion of missing data.

4.2 Impact of Skin Care Products on Microbiome Dynamics

In this example, researchers want to know how the skin microbiome would be altered when the hygiene routine is modified, and whether this alteration is similar across different body sites (Bouslimani et al., 2019). Twelve healthy subjects participated in this 9-week study,

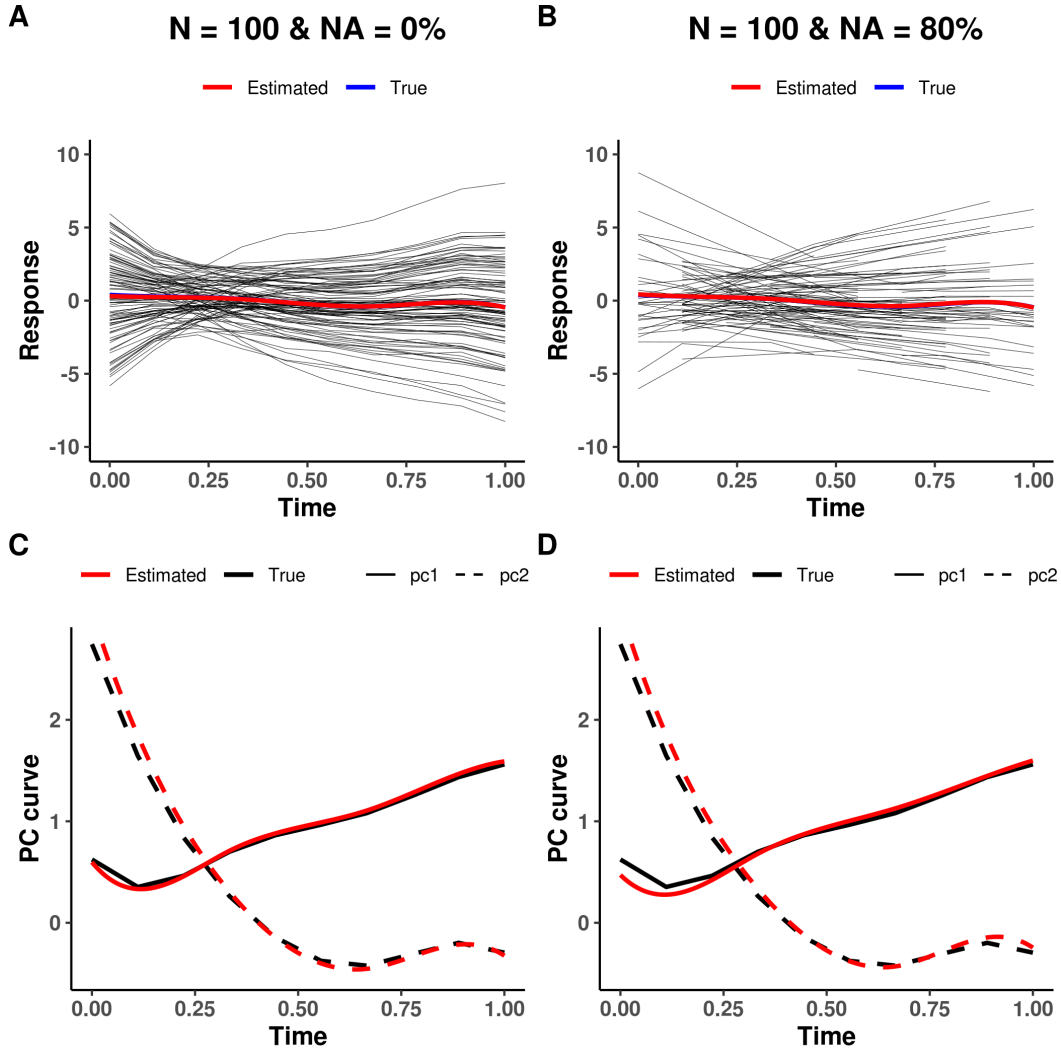


Figure 2: Results of Bayesian SFPCA on simulated data with 100 total samples of 0% vs. 80% missing data. (A) Estimated (red) vs. true (blue) overall mean curve on simulated trajectories (black) with 0% missing data. (B) Estimated (red) vs. true (blue) overall mean curve on simulated trajectories (black) with 80% missing data. (C) Estimated (red) vs. true (black) PC curves on simulated data with 0% missing data. (D) Estimated (red) vs. true (black) PC curves on simulated data with 80% missing data.

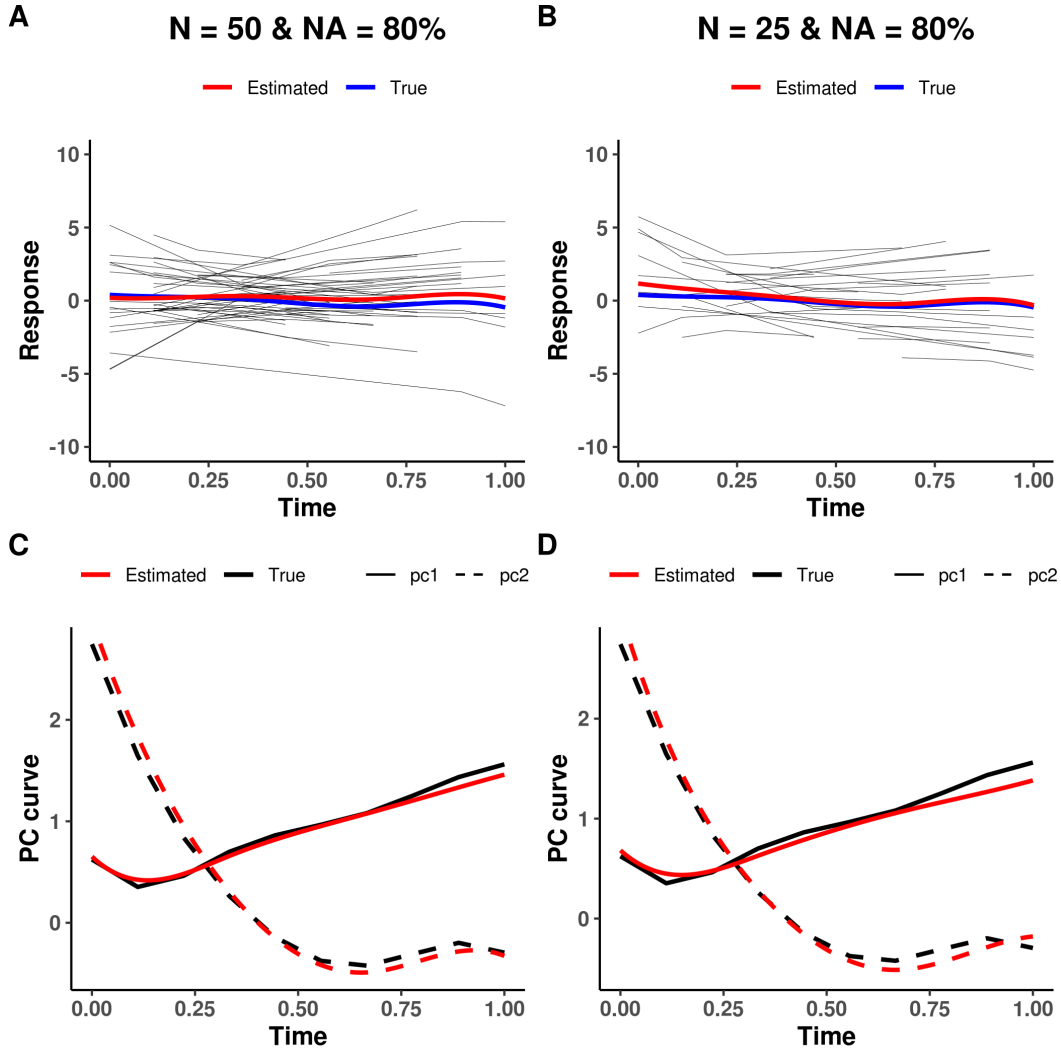


Figure 3: Results of Bayesian SFPCA on simulated data with 50 vs. 25 total samples of 80% missing data. (A) Estimated (red) vs. true (blue) overall mean curve on simulated trajectories (black) with 50 samples. (B) Estimated (red) vs. true (blue) overall mean curve on simulated trajectories (black) with 25 samples. (C) Estimated (red) vs. true (black) PC curves on simulated data with 50 samples. (D) Estimated (red) vs. true (black) PC curves on simulated data with 25 samples.

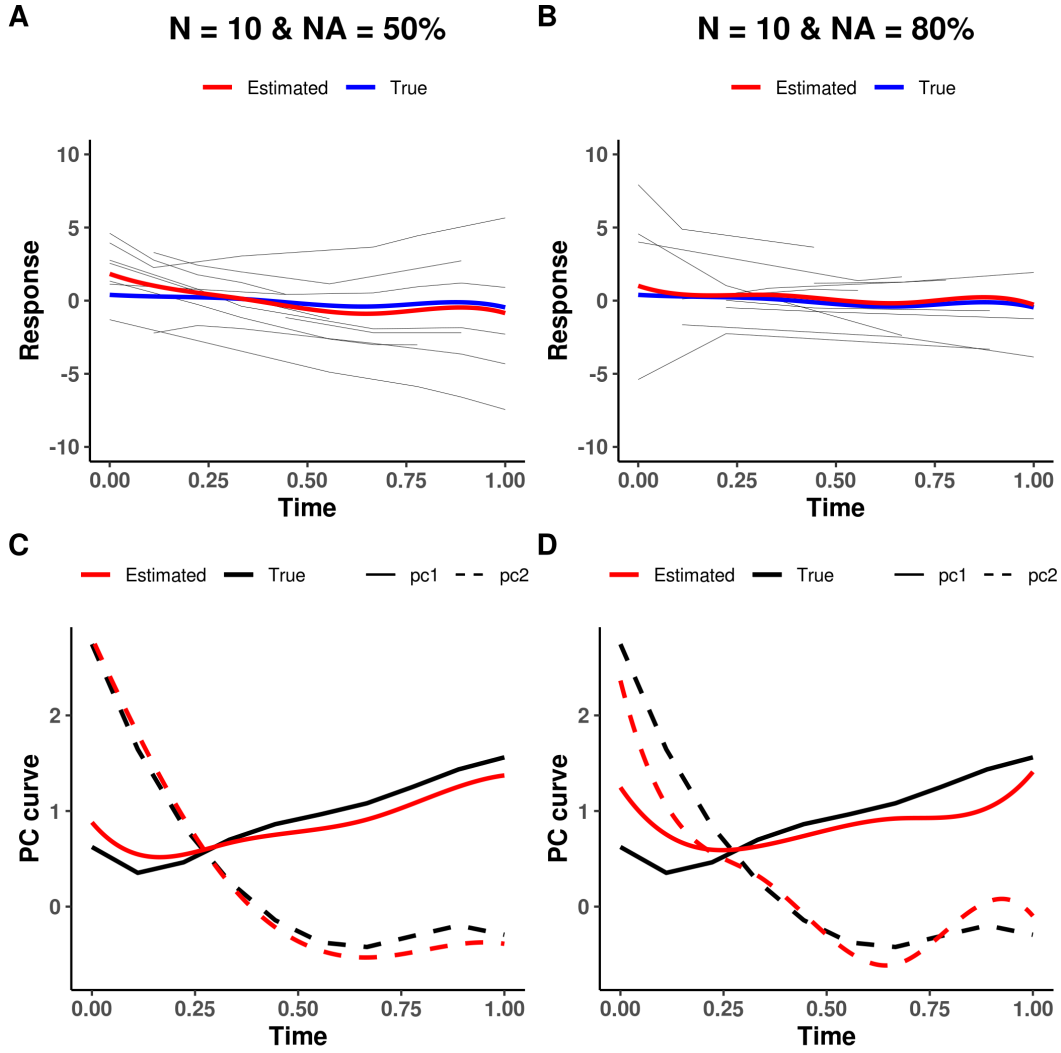


Figure 4: Results of Bayesian SFPCA on simulated data with 10 total samples of 50% vs. 80% missing data. (A) Estimated (red) vs. true (blue) overall mean curve on simulated trajectories (black) with 50% missing data. (B) Estimated (red) vs. true (blue) overall mean curve on simulated trajectories (black) with 80% missing data. (C) Estimated (red) vs. true (black) PC curves on simulated data with 50% missing data. (D) Estimated (red) vs. true (black) PC curves on simulated data with 80% missing data.

Table 1: Average mean squared errors with 95% CIs for estimating mean spline coefficients (θ_μ) in simulations with different sample size (N) and proportion of missing values (NA).

	N = 100	N = 50	N = 25	N = 20
NA = 0%	0.008 (0, 0.029)	0.015 (0, 0.066)	0.031 (0, 0.173)	0.044 (0.002, 0.188)
NA = 20%	0.008 (0, 0.034)	0.01 (0, 0.052)	0.021 (0.001, 0.088)	0.04 (0.001, 0.138)
NA = 50%	0.008 (0, 0.034)	0.011 (0, 0.053)	0.021 (0.001, 0.082)	0.041 (0.001, 0.154)
NA = 80%	0.007 (0, 0.025)	0.013 (0.001, 0.08)	0.026 (0.001, 0.105)	0.069 (0.009, 0.223)

Table 2: Average mean squared errors with 95% CIs for estimating FPC spline coefficients (Θ) in simulations with different sample size (N) and proportion of missing values (NA).

	N = 100	N = 50	N = 25	N = 20
NA = 0%	0.002 (0.001, 0.01)	0.011 (0.001, 0.116)	0.02 (0.001, 0.143)	0.049 (0.003, 0.21)
NA = 20%	0.002 (0.001, 0.005)	0.005 (0.001, 0.03)	0.018 (0.001, 0.157)	0.05 (0.003, 0.208)
NA = 50%	0.002 (0.001, 0.005)	0.005 (0.001, 0.026)	0.02 (0.001, 0.162)	0.054 (0.003, 0.203)
NA = 80%	0.004 (0.001, 0.016)	0.01 (0.001, 0.079)	0.027 (0.002, 0.208)	0.081 (0.017, 0.246)

and samples were collected from each individual on four skin body sites (face, armpits, front forearms and toes). For the baseline (week 0), subjects performed their normal routine of using their personal skin care products. During the first three weeks (w1-w3), all volunteers used only the same head-to-toe shampoo and no other product was applied. In the following 3 weeks (w4-w6), four selected commercial products were applied daily by all volunteers on the specific body site: sunscreen for the face, deodorant antiperspirant for the armpits, moisturizer for the front forearm, and soothing foot powder for the toes, and continued use of the same shampoo. For the last three weeks (w7-w9), all volunteers went back to their normal routine using their personal products. Due to its specific study design, the perturbations of the skin microbiome are expected to occur around the intervention time points. The outcome of interest in this example is the longitudinal pattern of Shannon microbial diversity of the microbiome, defined as $Shannon = -\sum_{i=1}^S p_i \ln(p_i)$, where S is the total number of species, and p_i is the relative proportion of species i relative to the entire population.

The best SFPCA model was selected by PSIS-LOO to have four PCs and three internal knots for the cubic spline basis. The estimated difference of expected leave-one-out prediction errors between the models with three and four PCs was smaller than the standard error, hence they could both be considered as adequate models. We chose the model with the highest value of $\widehat{elppd}_{psis-loo}$, which has four principal components and three internal knots. The model diagnostics using graphical posterior predictive checks showed that the simulated data from the posterior predictive distribution was able to cover the distribution of observed outcomes well (Figure 5A). Moreover, the estimated shape parameters from PSIS-LOO were all under the threshold of 0.7, except for one subject with a marginal value at 0.71 and another with an extreme value at 1.15 (Figure 5B). To examine these two potential outliers, we compared their observed trajectories with the predicted curves. Figure 5C, D showed that the observed trajectories (black) were closely followed by the predicted curves (red) and fell within the 95% credible intervals (blue). All these suggested that our selected SFPCA model was able to fit this dataset well.

As seen in Figure 6A, the population mean curve reveals an overall trend of an initial

decrease in microbial diversity during the first 3 weeks due to the cessation of using personal skin care products, an increase in the middle 3 weeks because of the introduction of four additional products, and a decrease toward the end due to the resumption of normal routines. Figure 6B shows the first four estimated PCs, with the first two PCs explaining over 90% of the variance. The first principal component captures variation in changes in microbial diversity around week 2.5 and week 5. The second component captures additional variation in changes around week 8. In Figure 6C-D, by adding a PC with ± 1 standard deviation of PC scores to the population mean curve, we illustrate how the first and second PCs impact the trajectories. The first PC represents an overall vertical shift of the mean microbial diversity, and explains about 80% of the variance. An individual with a high score on this component has on average higher microbial diversity than one with a lower score, and *vice versa*. The second PC curve explains 12% of the variance, and captures variation during the middle three weeks. Since a trajectory of each individual is represented as a weighted sum of these principal modes of variation, we can use each individual’s PC scores to gain insight about microbial perturbations in different body sites (Figure 6E-F). The scores of the first PC unveil the order of microbial diversity from highest to lowest in the four body sites, where arm has the highest diversity over time, while armpit the lowest. The signs of mean scores (positive or negative) indicate that arm and face share one similar temporal pattern, corresponding to the orange curve in Figure 6C, while foot and armpit share another temporal pattern, corresponding to the blue curve in Figure 6C. A similar temporal clustering of face and arm, versus foot and armpit was observed in scores of the second PC as well.

5 Discussion

We have introduced a Bayesian approach to SFPCA, providing users an efficient Bayesian model selection technique like PSIS-LOO and reliable model diagnostics methods such as examining the estimated shape parameters from PSIS-LOO and utilizing the graphical posterior predictive checks. Moreover, our Bayesian modeling approach is flexible in incorporating alternative prior distributions, for example, a t-distribution to capture heavy tails

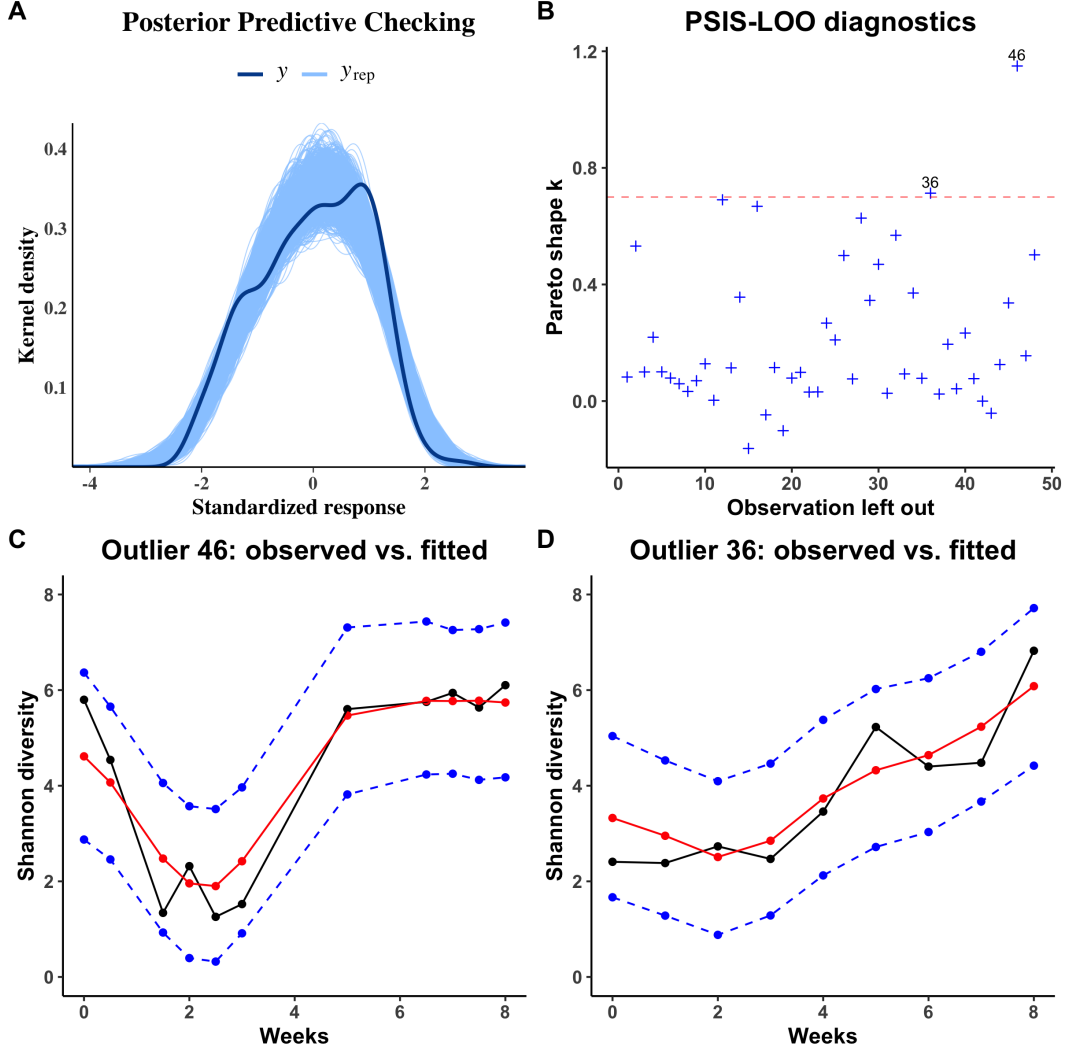


Figure 5: Graphical model diagnostics with posterior predictive checks and PSIS-LOO diagnostic plot for Bayesian SFPCA application to skin microbiome dataset. (A) Graphical posterior predictive checks: kernel density estimate of the observed dataset y (dark curve), with kernel estimates for 100 simulated dataset y_{rep} drawn from the posterior predictive distribution (thin, lighter lines). (B) Scatterplot of estimated Pareto shape parameter \hat{k} in PSIS-LOO diagnostic plot: all but two \hat{k} 's are lower than the warning threshold 0.7. (C) Observed (black), predicted (red) trajectories with 95% credible intervals (dashed blue lines) for potential outlier 46. (D) Observed (black), predicted (red) trajectories with 95% credible intervals (dashed blue lines) for potential outlier 36.

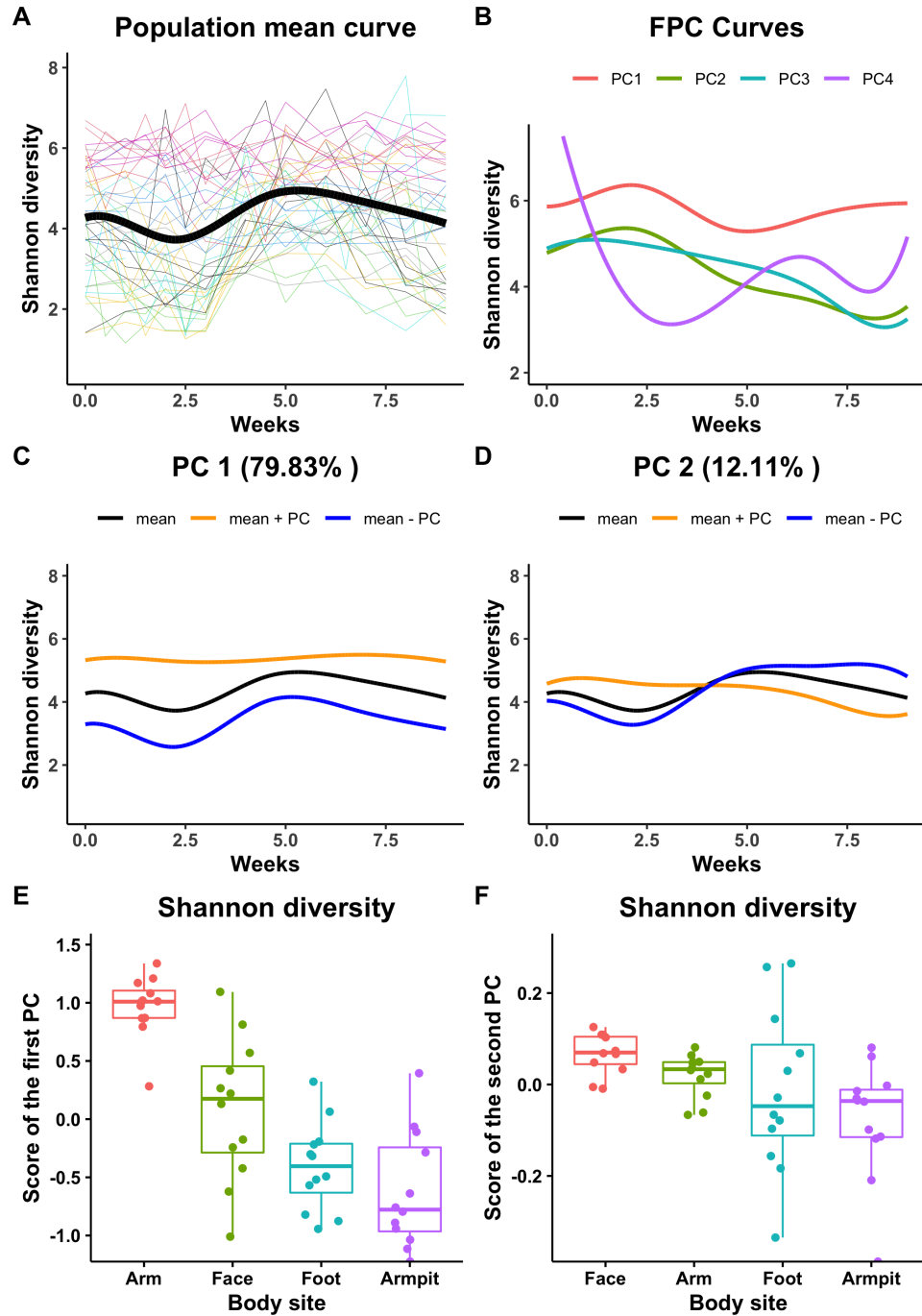


Figure 6: Results of Bayesian SFPCA on skincare impact microbiome dataset. (A) Estimated population mean curve (black) on observed individual trajectories (colored). (B) Trends of variability captured by 4 principal component curves. (C) Effects of adding (orange) and subtracting (blue) PC 1 with 1 SD of PC score to the population mean curve (black). (D) Effects of adding (orange) and subtracting (blue) PC 2 with 1 SD PC score to the population mean curve (black). (E) Progression trends based on PC 1 scores in different body sites. (F) Progression trends based on PC 2 scores in different body sites.

in the distribution of principal component scores α_i , which are easily implemented in **Stan**. The examples in Section 4 demonstrate the potential of this Bayesian approach to select the optimal model and uncover meaningful biological insights after careful model implementation and diagnostics. The first limitation of our current Bayesian SFPCA method is that it can only model one temporal measurement for different subjects over time, while microbiome data are typically comprised of thousands of microbes. This drawback would restrict the microbiome applications of this method to mainly analyses of alpha diversity, changes or differences in beta diversity, or measurement of a specific microbe. But given the flexibility in Bayesian modeling, it is feasible to extend the current model to multiple outcome measures simultaneously. The second limitation of our method is that the Bayesian implementation of SFPCA is less computationally efficient than frequentist approaches. However, with the goal of building more valid and reliable models in real data applications, our flexible modeling options, model selection and diagnostics with PSIS-LOO grants advantages over other available SFPCA approaches. Moreover, since the SFPCA model is implemented in **Stan**, a programming language with a very active user base, the **BayesTime** R package will be able to be updated with more efficient MCMC sampling algorithms and also incorporate other groundbreaking model selection and diagnostic techniques whenever they become available. Hence, we believe that the Bayesian approach to SFPCA will enable broader applications to a wider range of longitudinal data analysis going forward.

6 Acknowledgements

We thank Yoshiki Vázquez-Baeza, Tomasz Kościółek, and Antonio González for suggestions and insights on microbiome data analysis, and Jeff De Reus for advice on high performance computing.

LN was partially supported by funding from the National Institute of Health grants: NIDDK 1R01DK110541-01A1 and NIA 1P01AG052352-01A1. RK was supported by NIH under grant 1DP1AT010885, NIDDK under grant 1P30DK120515, and CCFA under grant 675191. WT was supported by NIH/NIMH under grants RF1 MH120025 and R01 MH122688.

References

- Bouslimani, A., da Silva, R., Kosciulek, T., Janssen, S., Callewaert, C., Amir, A., Dorrestein, K., Melnik, A. V., Zaramela, L. S., Kim, J.-N. et al. (2019), “The impact of skin care products on skin chemistry and microbiome dynamics,” *BMC biology*, 17, 1–20.
- Caporaso, J. G., Lauber, C. L., Costello, E. K., Berg-Lyons, D., Gonzalez, A., Stombaugh, J., Knights, D., Gajer, P., Ravel, J., Fierer, N. et al. (2011), “Moving pictures of the human microbiome,” *Genome biology*, 12, 1–8.
- Carpenter, B., Gelman, A., Hoffman, M. D., Lee, D., Goodrich, B., Betancourt, M., Brubaker, M., Guo, J., Li, P., and Riddell, A. (2017), “Stan: A probabilistic programming language,” *Journal of statistical software*, 76.
- David, L. A., Maurice, C. F., Carmody, R. N., Gootenberg, D. B., Button, J. E., Wolfe, B. E., Ling, A. V., Devlin, A. S., Varma, Y., Fischbach, M. A. et al. (2014), “Diet rapidly and reproducibly alters the human gut microbiome,” *Nature*, 505, 559–563.
- Dethlefsen, L., and Relman, D. A. (2011), “Incomplete recovery and individualized responses of the human distal gut microbiota to repeated antibiotic perturbation,” *Proceedings of the National Academy of Sciences*, 108, 4554–4561.
- Dominguez-Bello, M. G., De Jesus-Laboy, K. M., Shen, N., Cox, L. M., Amir, A., Gonzalez, A., Bokulich, N. A., Song, S. J., Hoashi, M., Rivera-Vinas, J. I. et al. (2016), “Partial restoration of the microbiota of cesarean-born infants via vaginal microbial transfer,” *Nature medicine*, 22, 250.
- Fierer, N., Hamady, M., Lauber, C. L., and Knight, R. (2008), “The influence of sex, handedness, and washing on the diversity of hand surface bacteria,” *Proceedings of the National Academy of Sciences*, 105, 17994–17999.
- Flores, G. E., Caporaso, J. G., Henley, J. B., Rideout, J. R., Domogala, D., Chase, J., Leff, J. W., Vázquez-Baeza, Y., Gonzalez, A., Knight, R. et al. (2014), “Temporal variability is a personalized feature of the human microbiome,” *Genome biology*, 15, 531.

- Gabry, J., Simpson, D., Vehtari, A., Betancourt, M., and Gelman, A. (2019), “Visualization in Bayesian workflow,” *Journal of the Royal Statistical Society: Series A (Statistics in Society)*, 182, 389–402.
- Gelfand, A. E., Dey, D. K., and Chang, H. (1992), “Model determination using predictive distributions with implementation via sampling-based methods,” Tech. rep., STANFORD UNIV CA DEPT OF STATISTICS.
- Gelman, A., Meng, X.-L., and Stern, H. (1996), “Posterior predictive assessment of model fitness via realized discrepancies,” *Statistica sinica*, 733–760.
- Gibson, T. E., and Gerber, G. K. (2018), “Robust and scalable models of microbiome dynamics,” *arXiv preprint arXiv:1805.04591*.
- Halfvarson, J., Brislawn, C. J., Lamendella, R., Vázquez-Baeza, Y., Walters, W. A., Bramer, L. M., D’amato, M., Bonfiglio, F., McDonald, D., Gonzalez, A. et al. (2017), “Dynamics of the human gut microbiome in inflammatory bowel disease,” *Nature microbiology*, 2, 1–7.
- James, G. M., Hastie, T. J., and Sugar, C. A. (2000), “Principal component models for sparse functional data,” *Biometrika*, 87, 587–602.
- Kidziński, L., and Hastie, T. (2018), “Longitudinal data analysis using matrix completion,” *arXiv preprint arXiv:1809.08771*.
- Kostic, A. D., Gevers, D., Siljander, H., Vatanen, T., Hyötyläinen, T., Hämäläinen, A.-M., Peet, A., Tillmann, V., Pöhö, P., Mattila, I. et al. (2015), “The dynamics of the human infant gut microbiome in development and in progression toward type 1 diabetes,” *Cell host & microbe*, 17, 260–273.
- McDonald, D., Hyde, E., Debelius, J. W., Morton, J. T., Gonzalez, A., Ackermann, G., Aksenov, A. A., Behsaz, B., Brennan, C., Chen, Y. et al. (2018), “American Gut: an open platform for citizen science microbiome research,” *Msystems*, 3, e00031–18.

- Méthé, B. A., Nelson, K. E., Pop, M., Creasy, H. H., Giglio, M. G., Huttenhower, C., Gevers, D., Petrosino, J. F., Abubucker, S., Badger, J. H. et al. (2012), “A framework for human microbiome research,” *nature*, 486, 215.
- Peng, J., and Paul, D. (2009), “A geometric approach to maximum likelihood estimation of the functional principal components from sparse longitudinal data,” *Journal of Computational and Graphical Statistics*, 18, 995–1015.
- Ramsay, J. O., and Silverman, B. W. (2007), *Applied functional data analysis: methods and case studies*, Springer.
- Ridenhour, B. J., Brooker, S. L., Williams, J. E., Van Leuven, J. T., Miller, A. W., Dearing, M. D., and Remien, C. H. (2017), “Modeling time-series data from microbial communities,” *The ISME journal*, 11, 2526–2537.
- Shenhav, L., Furman, O., Briscoe, L., Thompson, M., Silverman, J. D., Mizrahi, I., and Halperin, E. (2019), “Modeling the temporal dynamics of the gut microbial community in adults and infants,” *PLoS computational biology*, 15, e1006960.
- Silverman, J. D., Durand, H. K., Bloom, R. J., Mukherjee, S., and David, L. A. (2018), “Dynamic linear models guide design and analysis of microbiota studies within artificial human guts,” *Microbiome*, 6, 1–20.
- Silverman, J. D., Roche, K., Holmes, Z. C., David, L. A., and Mukherjee, S. (2019), “Bayesian multinomial logistic normal models through marginally latent matrix-t processes,” *arXiv preprint arXiv:1903.11695*.
- Smarr, L., Hyde, E. R., McDonald, D., Sandborn, W. J., and Knight, R. (2017), “Tracking human gut microbiome changes resulting from a colonoscopy,” *Methods of information in medicine*, 56, 442–447.
- Turnbaugh, P. J., Ley, R. E., Hamady, M., Fraser-Liggett, C. M., Knight, R., and Gordon, J. I. (2007), “The human microbiome project,” *Nature*, 449, 804–810.

- Turnbaugh, P. J., Ridaura, V. K., Faith, J. J., Rey, F. E., Knight, R.— (2009), “The effect of diet on the human gut microbiome: a metagenomic analysis in humanized gnotobiotic mice,” *Science translational medicine*, 1, 6ra14–6ra14.
- Vehtari, A., Gelman, A., and Gabry, J. (2017), “Practical Bayesian model evaluation using leave-one-out cross-validation and WAIC,” *Statistics and computing*, 27, 1413–1432.
- Vehtari, A., Simpson, D., Gelman, A., Yao, Y.— (2015), “Pareto smoothed importance sampling,” *arXiv preprint arXiv:1507.02646*.
- Weingarden, A., González, A., Vázquez-Baeza, Y., Weiss, S., Humphry, G., Berg-Lyons, D., Knights, D., Unno, T., Bobr, A., Kang, J. et al. (2015), “Dynamic changes in short-and long-term bacterial composition following fecal microbiota transplantation for recurrent *Clostridium difficile* infection,” *Microbiome*, 3, 1–8.
- Yao, F., Müller, H.-G., and Wang, J.-L. (2005), “Functional data analysis for sparse longitudinal data,” *Journal of the American statistical association*, 100, 577–590.
- Zhang, J., and Stephens, M. A. (2009), “A new and efficient estimation method for the generalized Pareto distribution,” *Technometrics*, 51, 316–325.